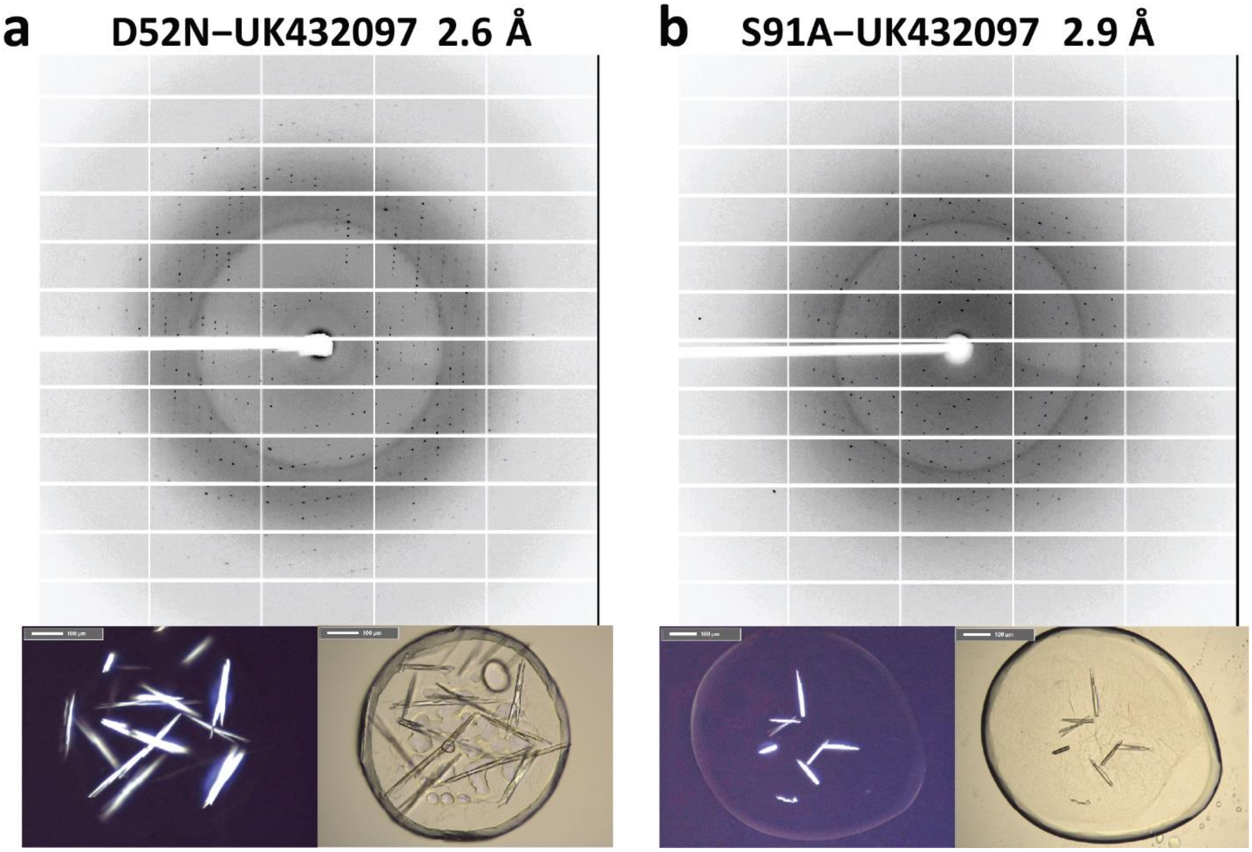

Figure S1. Related to Figure 2: **Diffraction pattern and crystals of D52N–UK432097 and S91A–UK432097**. Diffraction images of crystals of (a) D52N–UK432097 and (b) S91A–UK432097. Below each are representative images of crystals under cross-polarized and bright field magnification. The D52N–UK432097 crystals consistently grew larger and had higher quality diffraction than the S91A–UK432097. The scale bar is 100 µm.

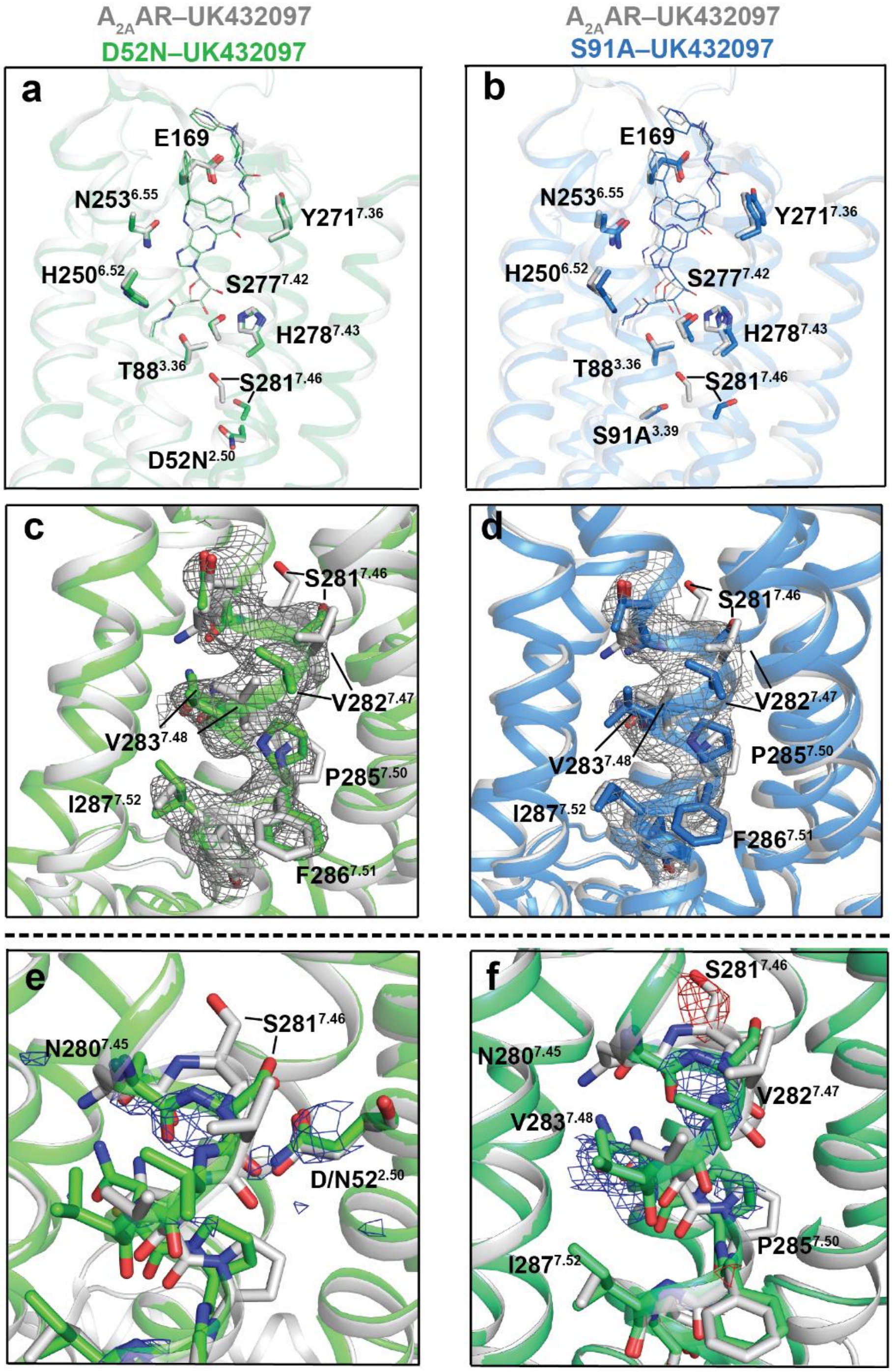

Figure S2. Related to Figure 2 and 3: **UK432097 binding pose and NPxxY electron density maps in D52N–UK432097 and S91A–UK432097**. UK432097 is shown as grey (A$_{2A}$AR-UK432097; PDB 3QAK), green (D52N–UK432097), or blue (S91A–UK432097) lines. Residues involved in ligand binding are highlighted as sticks with the same respective colorations.

Additional residues of interest were shown as stick representations; (a) D52$^{2.50}$N, (b) and S91$^{3.39}$A, and (a-b) S281$^{7.46}$. 2|F_o|-|F_c| electron densities (grey mesh) of the NPxxY motif for the (c) D52N–UK432097 and (d) S91A–UK432097 NPxxY motifs contoured at 1σ and carved at 1.8 Å. (e) The |F_o|-|F_c| electron density maps between D52N-UK432097 and A_{2A}AR-UK432097 (3QAK) (blue mesh) is contoured at 3σ and shows clear changes near S281$^{7.46}$ and at the site of mutation N52$^{2.50}$. (f) The |F_o|-|F_c| electron density maps for MR using 3QAK as a search model was contoured at 3σ for both positive (blue mesh) and negative (red mesh) densities and carved at 1.6 Å (f).

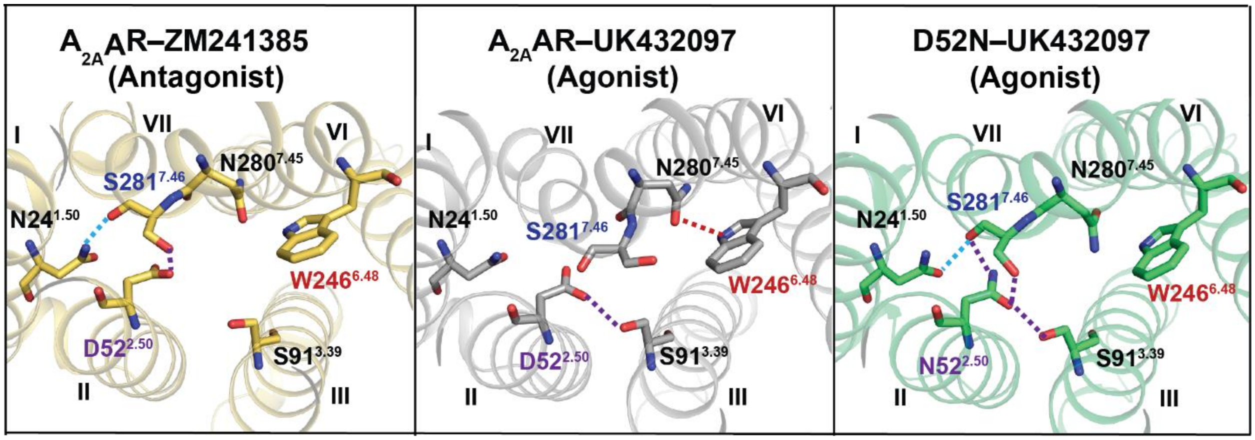

Figure S3. Related to Figure 5: Hydrogen bonding networks in A_{2A}AR–ZM241385, A_{2A}AR–UK432097, and D52N–UK432097. Comparison of structures of A_{2A}AR and A_{2A}AR-D52N complexes illustrating changes in the interhelical hydrogen bond network, relating to the schematic shown in Figure 5 of the main text. A_{2A}AR–ZM241385 is shown in yellow, A_{2A}AR–UK432097 is shown in grey, and D52N–UK432097 is shown in green.

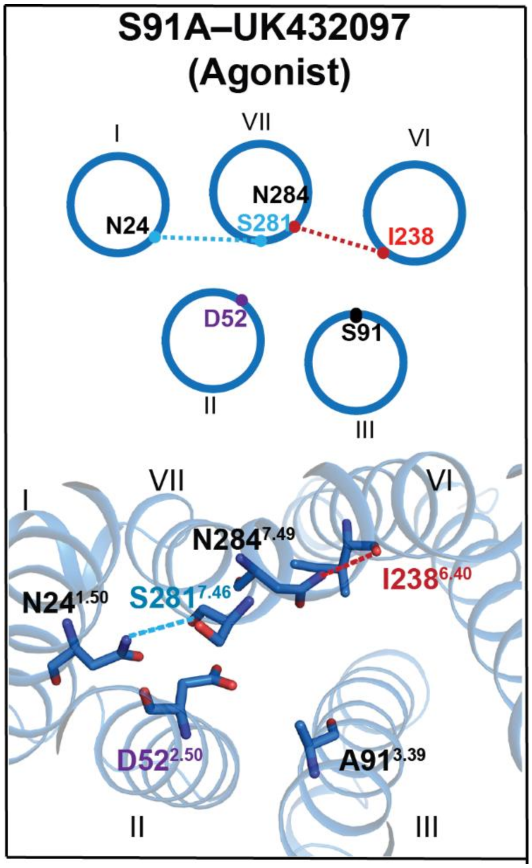

Figure S4. Related to Figure 5: **The hydrogen bonding networks of S91A–UK432097**. The top panel presents an intracellular view of helices I-III, VI, and VII, indicated by circles with Roman numerals. Amino acids involved in hydrogen bonding between helices are indicated by colored dots on each circle and labeled. Dashed lines between helices indicate the presence of a hydrogen bond. The bottom panel presents an intracellular view of the same helices shown in cartoon representation, and the same amino acids labeled in the top panels are shown in stick representation.

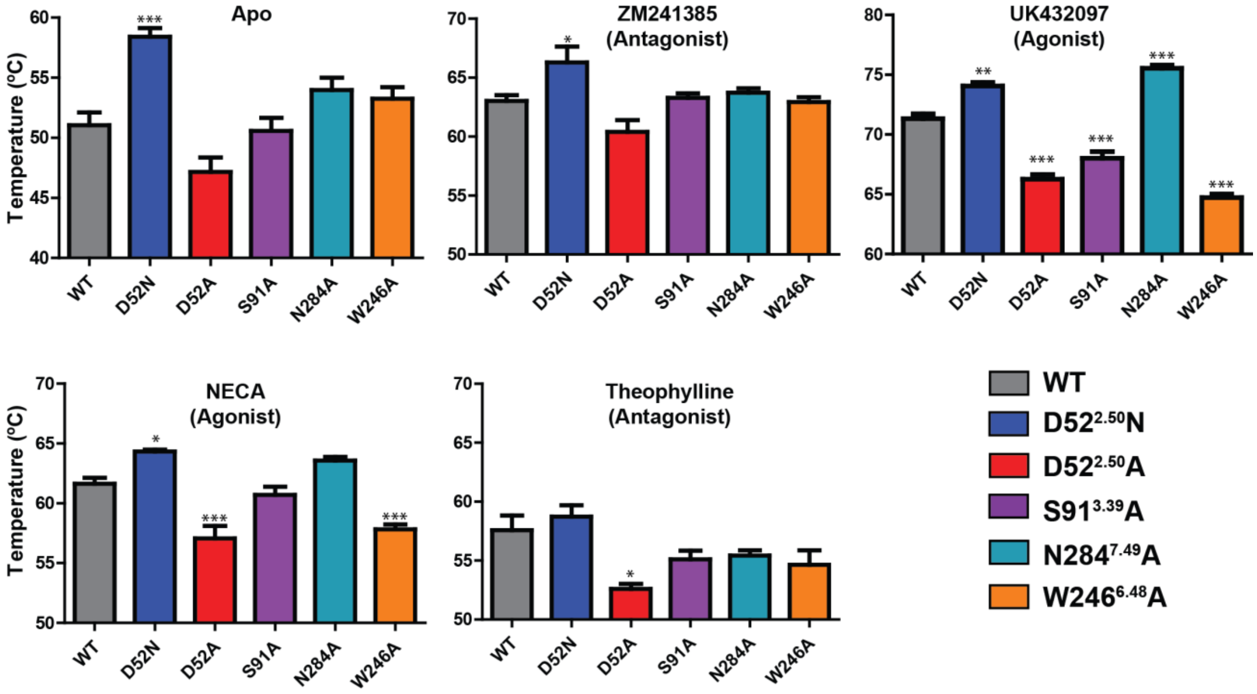

Figure S5. Related to Figure 6: Statistical analysis of A_{2A}AR variants on melting temperature values (T_m) from thermal shift assays. Melting temperature values plotted are means ± S.E.M. (n = 3 or more). Asterisks are used to indicate P-values associated with statistical analysis of the data: * $P < 0.05$, ** $P < 0.01$, and *** $P < 0.001$. Results were used to generate Figure 6a.

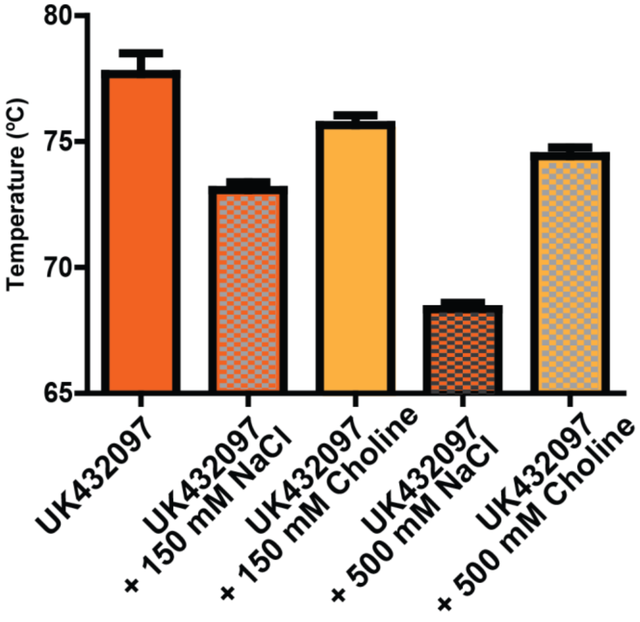

Figure S6. Related to Figure 6: The effect of sodium on melting temperatures of A_{2A}AR in complex with the agonist UK432097. Melting temperatures are shown as means ± S.E.M. (n = 3 or more), as determined by analysis of thermal shift assays for A_{2A}AR in complex with the full agonist UK432097 in the presence or absence of sodium chloride. For experiments in the absence of sodium chloride, choline chloride was present in the sample solution at the same concentration.

Table S1. Related to Figure 6

	Apo °C	ZM241385 °C	UK432097 °C	NECA °C	Theophylline °C
WT	50.89 ± 0.18	62.95 ± 0.15	71.33 ± 0.22	61.56 ± 0.12	57.64 ± 0.17
D52$^{2.50}$ N	58.35 ± 0.16	65.86 ± 0.19	74.05 ± 0.22	64.18 ± 0.10	58.58 ± 0.16
D52$^{2.50}$A	46.86 ± 0.39	59.86 ± 0.20	66.36 ± 0.29	57.57 ± 0.29	54.49 ± 0.23
S91$^{3.39}$A	50.10 ± 0.27	63.29 ± 0.08	67.94 ± 0.31	60.75 ± 0.16	55.11 ± 0.22
N284$^{7.49}$A	53.80 ± 0.22	63.63 ± 0.10	75.75 ± 0.22	63.50 ± 0.11	55.43 ± 0.13
W246$^{6.48}$A	53.00 ± 0.22	63.50 ± 0.09	64.68 ± 0.22	57.79 ± 0.10	54.09 ± 0.22

Melting temperature values (T_m) from thermal shift assays for A_{2A}AR variants with a panel of ligands. Values shown represent the means ± S.D. (n = 3 or more). This data was used to generate Figure 6a and Figure S5.